High-content screening identifies a critical role for P pili in early adhesion of uropathogenic Escherichia coli to bladder cells

Thomas Simonet (thomas.simonet@epfl.ch)
EPFL https://orcid.org/0000-0003-3259-4942
Ophélie Rutschmann
Swiss Federal Institute of Technology in Lausanne
Kunal Sharma
EPFL
Théo Nass
EPFL
Maria Pavlou
EPFL
Anaëlle Dubois
EPFL
Graham Knott
EPFL https://orcid.org/0000-0002-2956-9052
John McKinney
Swiss Federal Institute of Technology in Lausanne (EPFL) https://orcid.org/0000-0002-0557-3479

Article

Keywords: uropathogenic Escherichia coli (UPEC), bladder epithelial cells, bacterial adhesion, P pili, urinary tract infections (UTIs), transposon insertion library, high-content screening, scanning electron microscopy (SEM), surface proteomics

Posted Date: December 19th, 2022

DOI: https://doi.org/10.21203/rs.3.rs-2379019/v1

Abstract

Urinary tract infections (UTIs) caused by uropathogenic Escherichia coli (UPEC) are notoriously difficult to treat due to the ability of UPEC to adhere to and invade urothelial bladder cells. UPEC strains encode a variety of adhesins whose roles in adhesion and invasion are not fully elucidated. Using a transposon insertion library derived from the UPEC clinical isolate CFT073, we developed a high-content screening assay to identify UPEC mutants with defects in early adhesion to human bladder epithelial cells. Of a total of 8,184 mutants screened, we recovered 82 (1.0%) and 54 (0.7%) mutants with decreased and increased adhesion, respectively. Surprisingly, nine low-adhesion hits mapped to the two P pili operons encoded by CFT073, which are usually thought to mediate adhesion to kidney cells rather than bladder cells. These results were reinforced by examination of six high-adhesion hits mapping to the operon coding for F1C pili, where disruption of F1C pili function resulted in increased P pili synthesis. Taken together, these findings reveal a critical role for P pili in UPEC adhesion to bladder epithelial cells, which may inform the development of anti-adhesion therapies to prevent UTI recurrence.

Introduction

Urinary tract infections (UTIs) are among the most common infections in humans, with 50–60% of women and 13–14% of men developing a UTI at least once in their lifetime (Foxman et al., 2000; Foxman, 2002; Seminerio et al., 2011). Most community-acquired UTIs are initiated when bacteria originating from the fecal flora ascend the urethra and colonize the bladder lumen and tissue, leading to acute cystitis (Klein and Hultgren, 2020). In a small number of cases, bacteria ascend further through the ureters into the kidney, a condition known as pyelonephritis, which can quickly develop into life-threatening urosepsis (Katchman et al., 2005; Scholes et al., 2005; Nicolle, 2008). About 80% of community-acquired UTIs are caused by a heterogeneous group of uropathogenic *Escherichia coli* (UPEC) strains that are specifically adapted to colonizing the urinary tract (Foxman, 2010; Flores-Mireles et al., 2015). Due to the rapid development and spread of antimicrobial resistance among UPEC strains, UTIs have become increasingly difficult to treat, creating a significant societal and personal burden (Simmering et al., 2017). Even in the absence of clinically detectable antibiotic resistance, UTIs are characterized by high rates of recurrence, and it is estimated that 30% of patients experience a second infection within one year of resolution of their initial episode, despite receiving appropriate antibiotic treatment (Foxman, 2014; Lacerda Mariano et al., 2020). In the majority of cases, recurrent infections are caused by the same UPEC strain as the initial episode, suggesting UPEC persistence in the urinary tract (Ejrnaes et al., 2006; Stracy et al., 2022).

Persistence of UPEC within the urinary tract is thought to hinge on bacterial invasion of urothelial cells to establish an intracellular niche that protects against clearance by antimicrobial agents and the host immune system (Wiles et al., 2008; Lewis et al., 2016; Terlizzi et al., 2017; Blango and Mulvey, 2010). The currently accepted model of UPEC pathogenesis and persistence in the bladder is largely based on studies using mouse models of infection (Barber et al., 2016; Murray et al., 2021). Upon reaching the murine bladder lumen, UPEC adheres to superficial umbrella cells of the urothelium, which triggers its internalization (Mulvey et al., 1998; Martinez et al., 2000). Internalized bacteria proliferate rapidly to form

biofilm-like intracellular bacterial communities (IBCs) comprising hundreds to thousands of bacteria (Anderson et al., 2003; Duraiswamy et al., 2018). Efflux of bacteria from IBCs back into the bladder lumen results in infection of neighbouring umbrella cells, thus perpetuating the infection cycle (Justice et al., 2004; Iosifidis and Duggin, 2020; Sharma et al., 2021b). UPEC may also invade into deeper layers of the bladder urothelium and establish quiescent intracellular reservoirs (QIRs), which may be responsible for long-term bacterial persistence and recurrent infection (Mysorekar and Hultgren, 2006; Schwartz et al., 2011; Sharma et al., 2021a).

Adhesion of UPEC to the umbrella cells lining the bladder lumen is a necessary prelude to invasion of urothelial cells and formation of IBCs and QIRs, as it prevents mechanical elimination of bacteria by the bulk flow of urine (Bien et al., 2012; Flores-Mireles et al., 2015). In recent years, novel therapeutic strategies targeting UPEC adhesion have emerged as an exciting alternative to conventional antibiotic therapy (Spaulding et al., 2017; Sarshar et al., 2020). Bacteria assemble a wide variety of structures to mediate adhesion to surfaces, including pili, also known as fimbriae (Pizarro-Cerda and Cossart, 2006; Kline et al., 2009). Among pathogenic Gram-negative bacteria, the family of chaperone-usher pili (CUP) mediates most of the interactions with host cells, with a tissue tropism determined by the tip adhesin (Waksman and Hultgren, 2009; Thanassi et al., 2012). The collective pangenome of UPEC strains has been shown to harbour at least 38 distinct CUP operons, and genomes of individual UPEC strains often encode several of them, providing bacteria with the ability to bind to a variety of receptors and surfaces (Wurpel et al., 2013).

The genome of the well-studied UPEC clinical isolate CFT073 contains 10 CUP operons (Welch et al., 2002), among which type 1 pili and P pili play key roles in colonization of the bladder and kidney, respectively. Type 1 pili are thought to mediate UPEC adhesion in the bladder via binding of the FimH tip adhesin to mannosylated uroplakin residues on the surface of bladder umbrella cells (Mulvey et al., 1998; Martinez et al., 2000; Hung et al., 2002; Wright et al., 2007), while P pili are thought to mediate UPEC adhesion in the kidney via binding of the PapG tip adhesin to globoside glycolipids on the surface of kidney epithelial cells (Roberts et al., 1994; Dodson et al., 2001; Johnson et al., 2005; Lane et al., 2007; Lillington et al., 2014). In addition to type 1 and P pili, recent studies have implicated several other types of pili in adhesion to urothelial cells, including F9 pili, Yad pili, and Ygi pili (Wurpel et al., 2014; Conover et al., 2016; Spurbeck et al., 2011). However, the contribution of different types of pili to adhesion has so far mostly been assessed using laboratory strains of *E. coli* that recombinantly express one type of pili, rather than fully virulent UPEC strains that can simultaneously express several types of pili. It is also important to note that conventional adhesion assays are based on counting colony-forming units (CFU) in lysates of infected host cells, which does not distinguish between surface-adherent bacteria and internalized bacteria.

Here, we use high-throughput fluorescence microscopy-based screening to identify genes that contribute to early adhesion of the UPEC clinical isolate CFT073 to human bladder epithelial cells before bacterial invasion occurs. By screening a library of 8,184 random transposon insertion mutants, we identified 82 (1.0%) low-adhesion mutants and 54 (0.7%) high-adhesion mutants. Unexpectedly, none of the low-

adhesion transposon hits mapped to the operon coding for type 1 pili, whereas nine independent hits were identified in the two P pili operons encoded by CFT073. Consistent with these results, we found that early adhesion was reduced by deletion of either P pili operon, with deletion of both operons having an additive effect, while deletion of the type 1 pili operon had no effect. We also identified six high-adhesion mutants with independent transposon hits in the F1C pili operon, and we found that deletion of the entire F1C pili operon resulted in upregulation of both P pili operons without altering expression of the type 1 pili operon. Taken together, these results identify a previously unsuspected role for P pili in early adhesion of UPEC to the bladder epithelium, which may have important implications for the development of new therapies targeting bacterial adhesion in the bladder.

Results

A fluorescence microscopy-based assay quantifies early adhesion of UPEC to bladder epithelial cells in high throughput

We developed a high-throughput fluorescence microscopy-based assay to monitor early adhesion of UPEC to human bladder epithelial cells (Fig. 1A). The UPEC clinical isolate CFT073 was engineered to express sfGFP from a constitutive promoter integrated on the chromosome. Swimming motility was eliminated by deleting the *fliC* gene encoding flagellin in order to facilitate imaging and mass spectrometry analysis of the bacterial surface proteome (Materials and Methods). Human 5637 bladder epithelial cells were grown in 96-well plates and spinfected with bacteria at a multiplicity-of-infection (MOI) of 200:1. We confirmed by immunofluorescence that these cells expressed cytokeratin 8 (CK8) and uroplakin IIIa (UPK3A), which are markers for superficial umbrella cells of the bladder urothelium (Supplementary Figure S1). Importantly, uroplakin is thought to mediate UPEC colonization of the bladder through its terminal mannosyl moieties, which serve as receptors for type 1 pili (Wu et al., 1996; Zhou et al., 2001; Thumbikat et al., 2009). In order to focus on the initial stages of bacterial adhesion, rather than downstream events such as invasion and intracellular growth, spinfected plates were incubated at 37°C for only 20 minutes, then washed to remove non-adherent bacteria and immediately imaged (Fig. 1A). Automated microscopy was used to measure GFP fluorescence in each well as a proxy for the number of adherent bacteria, and the integrity of the epithelial cell layer was simultaneously assessed on the phase-contrast channel. We confirmed by scanning electron microscopy (SEM) that bacteria adhered to the surface of bladder cells using pili (Fig. 1B,C).

High-content screening identifies UPEC mutants with altered adhesion to bladder epithelial cells

The CFT073 sfGFP Δ*fliC* strain (hereafter Δ*fliC*) served as the parental strain for transposon mutagenesis. A library of 8,184 transposon mutants was screened following the procedure outlined in Fig. 1A, corresponding to about 80% saturation of the genome of CFT073, which is 5.2 Mb in length and contains 5,533 annotated protein-coding genes (Zilsel et al., 1992; Welch et al., 2002). Mutants that displayed decreased (Fig. 1E,G) or increased (Fig. 1F,G) adhesion to bladder epithelial cells compared to

the Δ*fliC* parental strain (Fig. 1D,G) were selected using an automated three-step screening procedure (Supplementary Figure S2). We identified and confirmed 82 low-adhesion mutants (1.0% of the total screened), representing 60 genes, and 54 high-adhesion mutants (0.7%), representing 32 genes (Supplementary Table S1). The positions of the transposon insertion sites within the genome of CFT073 were scattered throughout the chromosome with no obvious “hot spots” or “cold spots” (Supplementary Figure S3A).

Early adhesion of UPEC to bladder epithelial cells is differentially regulated by multiple genes

In order to establish pathways involved in early adhesion of UPEC to bladder epithelial cells, genes identified in the screen were grouped according to their KEGG (Kyoto Encyclopaedia of Genes and Genomes) classification. We focused in particular on genes with multiple independent hits and genes belonging to the same operon (Fig. 2). Most of the transposon insertions corresponding to high-adhesion phenotypes clustered within genes involved in biogenesis of the cell envelope (Fig. 2A). Specifically, operons linked to the synthesis of the lipopolysaccharide (LPS) O-antigen (Fig. 2A-1), the LPS core (Fig. <link rid="fig4">2</link>A-2), and the capsule layer (Fig. 2A-3) were repeatedly identified, possibly because trimming of these outward-facing surface structures results in enhanced pili display, as suggested previously (Schembri et al., 2004; Beloin et al., 2006). Interestingly, we also identified six insertions within the operon coding for the synthesis of F1C pili (Fig. 2A-4), which may suggest cross-regulation between different pili operons (Holden and Gally, 2004), resulting in upregulation of other adhesins in the absence of F1C pili (see below).

A number of low-adhesion mutants were linked to bacterial metabolism (Fig. 2B), especially energy metabolism, with several transposon hits identified within the operons coding for the components of the ATP synthase (Fig. 2B-5) and the cytochrome bd (Fig. 2B-6). We also identified genes associated with tRNA biogenesis and membrane transport, including the Pst ABC transporter for inorganic phosphate (Fig. 2B-7). Surprisingly, we did not identify a single hit directly linked to the synthesis of type 1 pili, which are thought to be the main mediators of UPEC adhesion to bladder cells (Martinez et al., 2000; Hung et al., 2002). However, we identified nine independent transposon insertions within genes coding for the synthesis of P pili (Fig. 2B-8), which are usually thought to be important primarily for colonization of the kidney in cases of pyelonephritis (Roberts et al., 1994; Dodson et al., 2001; Johnson et al., 2005; Lane et al., 2007; Lillington et al., 2014). Since the results from our screen identified a key role for P pili, but not for type 1 pili, in early adhesion of UPEC to bladder epithelial cells, we performed a series of additional assays to dissect the contribution of both types of pili to bacterial adhesion.

P pili are key mediators of early adhesion of UPEC to bladder epithelial cells

CFT073 encodes two P pili operons that are located on pathogenicity islands next to the tRNA genes *pheV* (hereafter referred to as the *pap1* operon encoding P1 pili) and *pheU* (hereafter referred to as the *pap2* operon encoding P2 pili) (Welch et al., 2002; Lloyd et al., 2007). Both operons have the same

organization, except for the regulatory gene *papX*, which is absent from *pap2* (Supplementary Figure S3B). Because of the high degree of sequence identity between corresponding genes of the two operons (Supplementary Figure S3B), the single-primer PCR protocol we used for mutant identification failed to assign transposon insertions to either *pap1* or *pap2*. We therefore developed a PCR assay that takes advantage of the distinct DNA sequences flanking the two operons (see Materials and Methods). Among the nine transposon insertions identified within P pili genes, eight were assigned to *pap1* and only one to *pap2*, within the *papF_2* coding sequence (Fig. 3A). All nine insertions led to an intermediate yet significant low-adhesion phenotype, which was most pronounced for insertions in *papF* and *papF_2* (Fig. 3B; Supplementary Figure S4).

We further assessed the contribution of each *pap* operon to UPEC adhesion by constructing unmarked deletion mutants of *pap1* and *pap2* in both the Δ*fliC* and wild-type backgrounds. The Δ*fliC* Δ*pap1* and Δ*fliC* Δ*pap2* strains both displayed an intermediate but significant adhesion defect, in agreement with the phenotypes of the corresponding transposon insertion mutants (Fig. 3C,D,E,F). The double *pap* deletion mutant Δ*fliC* Δ*pap1* Δ*pap2* displayed strongly impaired adhesion that was significantly greater than the adhesion defect of either single *pap* deletion mutant (Fig. 3C,D,G), indicating an additive role for *pap1* and *pap2* in adhesion to bladder cells. The low-adhesion phenotypes of the Δ*fliC pap* mutants were recapitulated when the single and double *pap* operon deletions were introduced in the wild-type (*fliC*$^{+}$) background (Supplementary Figure S5). These results confirm that loss of FliC does not affect early adhesion of UPEC to bladder epithelial cells in our assay, and underscore the critical role of P pili in this phenotype.

Expression of P pili, but not of type 1 pili, is upregulated in F1C UPEC mutants

We identified five transposon insertions within effector genes of the F1C pili operon (*focA*, *sfaD*, *focC*, and *focD*) and one insertion in the linked regulatory gene *sfaB*, which all led to a significant increase in UPEC adhesion to bladder cells (Fig. 4A; Supplementary Figure S6). This high-adhesion phenotype was recapitulated when we constructed an unmarked deletion mutant of the entire *foc* operon in the Δ*fliC* (Fig. 4B,C,D) or wild-type (Supplementary Figure S7) background, although the magnitude of the effect was more modest in the latter. Based on these results and the previous, we hypothesized that loss of F1C pili might lead to increased synthesis of P pili, resulting in increased adhesion of the *foc* mutants to bladder epithelial cells.

We tested this hypothesis by measuring the expression of genes corresponding to the major pilin subunits of type 1 pili (*fimA*), P1 pili (*papA*), and P2 pili (*papA_2*) in the Δ*fliC* Δ*foc* mutant strain. We observed a three-fold increase in *papA* expression and a two-fold increase in *papA_2* expression in the Δ*fliC* Δ*foc* strain compared to the Δ*fliC* parental strain, while expression of *fimA* was unaffected (Fig. 4E). Considering the high degree of sequence similarity between the different pilin genes (Supplementary Figure S3B), we confirmed the specificity of our assay by measuring pilin gene expression in the Δ*fim*, Δ*pap1*, and Δ*pap2* operon deletion mutants. As expected, in each operon deletion

mutant, expression of the corresponding pilin gene was abolished while expression of the two other pilin genes was unchanged (Fig. 4E).

To further assess whether increased *papA* and *papA_2* expression in the Δ*fliC* Δ*foc* mutant translates into increased P pili synthesis, we performed quantitative mass spectrometry analysis of the bacterial surface proteome. Surface-exposed proteins were isolated through surface biotinylation and protein affinity-purification (Monteiro et al., 2018). We confirmed that this procedure led to significant enrichment of proteins localized in the outer membrane based on gene ontology (GO) annotation of the CFT073 genome (Supplementary Figure S8A). In agreement with results of mRNA analysis (Fig. 4E), we observed a higher abundance of P1 and P2 pili proteins in the Δ*fliC* Δ*foc* mutant compared to the Δ*fliC* parental strain, while type 1 pili proteins did not show differential abundance between the two strains (Fig. 4F). Despite the similarity between P1 and P2 pili proteins (Supplementary Figure S3B), we verified that the Δ*pap1* and Δ*pap2* mutants could be distinguished at the protein level, inasmuch as PapA and PapG were decreased specifically in the Δ*fliC* Δ*pap1* strain, while PapA_2 and PapG_2 were decreased specifically in the Δ*fliC* Δ*pap2* strain (Supplementary Figure S8B,C). Overall, these results demonstrate increased synthesis of both P1 and P2 pili (but not type 1 pili) in the Δ*fliC* Δ*foc* mutant compared to the Δ*fliC* parental strain, consistent with evidence of cross-regulation between different pili operons in UPEC (Holden and Gally, 2004).

Type 1 pili are essential for invasion of UPEC into bladder epithelial cells even though they are not required for initial adhesion

Type 1 pili proteins were readily identified by mass spectrometry analysis of the UPEC surface proteome (Fig. 4F), confirming that type 1 pili were displayed on the bacterial cell surface. We obtained further support for this conclusion by developing an Ilastik-based image analysis pipeline to quantify piliation on SEM images of single bacterial cells (see Materials and Methods; Supplementary Figure S9). Compared to the Δ*fliC* parental strain (Fig. 5A,B), piliation was unchanged in the Δ*fliC papG*-Tn mutant (Fig. 5A,C) but was decreased in the Δ*fliC papC*-Tn mutant (Fig. 5A,D), in accordance with the disparate roles of PapG as the tip adhesin and of PapC as the usher component of the P1 pili assembly machinery. Consistent with this interpretation, we found that deletion of the entire P1 pili operon (Fig. 5A,E) or P2 pili operon (Fig. 5A,F) resulted in significantly decreased piliation compared to the parental strain. Similarly, deleting the entire type 1 pili operon led to a significant reduction in piliation (Fig. 5A,H), whereas deleting only the *fimH* gene encoding the type 1 pili tip adhesin had no effect (Fig. 5A,G). Taken together, these results confirm that type 1 pili are expressed on the cell surface of UPEC. Thus, absence of type 1 piliation cannot be the reason for our failure to identify transposon hits in the *fim* operon in our genetic screen.

We further investigated the role of type 1 pili in early adhesion of UPEC to bladder epithelial cells by recording the adhesion phenotypes of Δ*fim* deletion mutants constructed in both the wild-type and Δ*fliC* backgrounds. Consistent with the results of our screen, neither the Δ*fim* nor the Δ*fliC* Δ*fim* strain displayed a significant defect in adhesion to bladder epithelial cells (Fig. 5I,J,K; Supplementary Figure S10A,B,C,E). To rule out the possibility that loss of type 1 pili might be compensated by cross-regulation

of other pili operons as a consequence of deleting the entire *fim* operon, we demonstrated that adhesion was unaffected by deletion of *fimH* alone in both the wild-type (Fig. 5I,J,L) and Δ*fliC* (Supplementary Figure S10A,B,D,E) backgrounds. Overall, these results confirm that type 1 pili are not required for early adhesion of UPEC to bladder epithelial cells.

Since we did not identify a role for type 1 pili in early adhesion of UPEC to bladder cells, we asked whether we could confirm a role in UPEC internalization at later stages of infection (Anderson et al., 2003; Duraiswamy et al., 2018). Using a standard gentamicin protection assay to distinguish between extracellular and intracellular bacteria at 2 hours post-infection (see Materials and Methods), we indeed found that deletion of *fimH* or the entire *fim* operon led to reduced invasion of bladder epithelial cells by UPEC in the wild-type (Supplementary Figure S10F) and Δ*fliC* (Fig. 5M) backgrounds. These results suggest that in a UPEC strain expressing both type 1 and P pili, the essential role of type 1 pili in bladder cell invasion may not be initial adhesion *per se* but rather some downstream event.

Discussion

Adhesion of UPEC to superficial bladder umbrella cells is an essential prerequisite for the formation of biofilm-like intracellular bacterial communities (IBCs) and quiescent intracellular reservoirs (QIRs), which are thought to contribute to bacterial persistence within the bladder and recurrence of UTIs after appropriate antibiotic therapy (Justice et al., 2004; Mysorekar and Hultgren, 2006). As an alternative to conventional antibiotics, there is therefore a growing interest in developing anti-adhesion therapies for UTIs, which calls for a more complete understanding of the molecular mechanisms that promote bacterial adhesion to the bladder epithelium. Here, we perform unbiased high-content screening to identify genes that are important for early adhesion of a clinical UPEC isolate to human bladder epithelial cells. Unexpectedly, neither the results of our screen nor targeted analysis of unmarked deletion mutants support a role for type 1 pili in early adhesion of UPEC to bladder cells. Instead, our results highlight a critical role for P pili in early adhesion: deletion of genes encoding P pili leads to decreased adhesion to bladder cells, while deletion of genes encoding F1C pili leads to increased P pili synthesis and increased adhesion.

Type 1 pili are a well-established virulence factor in UPEC. Binding of type 1 pili to uroplakins expressed on the surface of bladder epithelial cells has been characterized in depth (Wu et al., 1996; Zhou et al., 2001; Thumbikat et al., 2009), and the contribution of type 1 pili to invasion of bladder epithelial cells has been documented in several studies, using both *in vivo* mouse UTI models and *in vitro* human cell culture-based systems (Mulvey et al., 1998; Martinez et al., 2000; Hung et al., 2002; Wright et al., 2007). In previous studies however, prolonged infection of bladder cells with UPEC did not permit the distinction between surface-adherent vs. internalized bacteria. Using a clinical isolate of UPEC, which simultaneously expresses a variety of pili types at the population level, we found that P pili play a dominant role in early adhesion to bladder epithelial cells, while type 1 pili are important for subsequent internalization. Our findings are consistent with previous studies performed in K12 laboratory strains of *E. coli* recombinantly expressing either type 1 or P pili. While recombinant bacteria were able in both cases to adhere to 5637

human bladder epithelial cells after two hours of co-incubation, only bacteria expressing type 1 pili were recovered after treatment of the infected cells with gentamicin (Martinez et al., 2000), indicating that expression of P pili by K12 was sufficient to mediate adhesion but not invasion. As an alternative strategy to distinguish between adherent vs. internalized bacteria, Virkola et al. tested the ability of recombinant K12 strains expressing either type 1 or P pili to adhere to fixed tissue sections from human bladder biopsies. After brief incubation, P-piliated bacteria adhered to the fixed tissue while type 1-piliated bacteria did not, indicating that expression of P pili by K12 was sufficient to mediate adhesion even under non-physiological conditions.

Although an essential role for type 1 pili in colonization of the bladder has been clearly demonstrated in mouse models of infection (Wright et al., 2007; Kalas et al., 2017), the evidence implicating type 1 pili in bladder colonization in humans is somewhat mixed (Hannan et al., 2012). Possible explanations for this apparent discrepancy include the fact that type 1 pili genes are variably expressed during UTIs in humans and only weakly expressed in human urine *in vitro* (Hagan et al., 2010; Subashchandrabose et al., 2014; Greene et al., 2015). Type 1 pili may also be bound by the Tamm-Horsfall protein, which has been shown to inhibit adhesion of type 1-piliated *E. coli* to uroplakins (Pak et al., 2001; Bates et al., 2004), or by uromodulin, which was recently shown to aggregate type 1-piliated bacteria, possibly facilitating their clearance from the urinary tract (Weiss et al., 2020). These observations suggest that type 1 pili might not be the only mediators of UPEC adhesion in the human bladder. Although it is generally thought that P pili are important for UPEC adhesion in the kidney rather than in the bladder, our demonstration of an essential role for P pili in early adhesion of CFT073 to bladder epithelial cells *in vitro* is consistent with evidence that P pili are expressed by UPEC in the human bladder *in vivo* (de Ree et al., 1987; Agata et al., 1989). Taken together, our findings therefore identify P pili as a potential new target in the development of treatment strategies to inhibit adhesion of pathogens to bladder epithelial cells early in the infection process.

The work presented here uncovers several other potential targets for the development of novel anti-adhesion therapies. Of note, the periplasmic chaperone DsbA, identified by several low-adhesion hits in our screen, was the target of a recent study aimed at identifying and evaluating small-molecule inhibitors as candidates for anti-virulence therapeutics in UPEC (Verderosa et al., 2021). DsbA is responsible for disulfide bond formation in pili subunits within the bacterial periplasm, and deletion of *dsbA* was previously shown to abolish P pili biogenesis in a laboratory strain of *E. coli* engineered to express P pili (Jacob-Dubuisson et al., 1994). Another example is the Dam DNA adenine methylase, also identified by several low-adhesion hits in our screen. Dam regulates several virulence factors and has been shown to be essential for epigenetic regulation of *fim*, *pap*, and *foc* transcription along with leucine-responsive regulatory protein Lrp and cAMP receptor protein Crp (van der Woude and Bäumler, 2004; Totsika et al., 2008), both of which were also identified as low-adhesion hits in our screen. With some modifications, our screening method could be used for other applications, for example, screening of small-molecule compound libraries to identify inhibitors of bacterial adhesion, or high-throughput analysis of collections of clinical isolates to compare their adhesion properties. These studies would not only advance our understanding of key mechanisms of UPEC pathogenesis in the bladder, they might also inform new

strategies for the development of small molecules targeting virulence factors as an alternative to conventional antibiotics.

Declarations

Acknowledgements

This research was supported by grants to J.D.M. from the Swiss National Science Foundation (SNSF, grant number 310030B_176397) and the National Centre of Competence in Research (NCCR) AntiResist funded by the SNSF (grant number 51NF40_180541). We thank Nicolas Chiaruttini, José Artacho, Romain Guiet, Olivier Burri, and Arne Seitz of the EPFL Bioimaging & Optics Core Facility for their assistance with high-content imaging. We thank Jonathan Pittet, Romain Hamelin, and Florence Armand of the EPFL Proteomics Core Facility for their help in optimizing the protocol for mass spectrometry analysis of the bacterial surfaceome. We thank Stéphanie Rosset, Marie Croisier, and Arnault Monoyer of the EPFL Biological Electron Microscopy Facility for their help in optimizing the SEM protocol for pili quantification. We thank Gabriel Bunke for his help in developing the high-content screening assay. We thank François-Signorino-Gelo and Neeraj Dhar for help with construction of the transposon mutant library. We thank Vivek V. Thacker, Chiara Toniolo, Gaëlle Vuaridel-Thurre, Kathrin Tomasek, and Richa Mishra for fruitful discussions and feedback on the manuscript. We thank and credit BioRender.com for the schematics presented in Fig. 1A.

Author contributions

T.M.S., K.S. and J.D.M. conceived the study. T.M.S. and K.S. designed experiments. T.M.S., O.R., T.N. and K.S. performed experiments. T.M.S. analysed data. T.M.S. constructed bacterial strains. M.P.P. analysed mass spectrometry data. A.D. and G.W.K. developed the Ilastik-based pipeline. T.M.S. and J.D.M. wrote the manuscript.

Materials And Methods

Plasmids and primers

Plasmids and primers used in this work are listed in Supplementary Tables S2 and S3, respectively. qRT-PCR primers are listed in Supplementary Table S5.

Human bladder epithelial cell culture

Human 5637 bladder epithelial cells (HTB-9™, procured from ATCC) were cultured in RPMI 1640 medium (ATCC) supplemented with 10% Fetal Bovine Serum (FBS, Gibco) at 37°C, 5% CO_2. Cells were split every other day by gentle detachment with trypsin-EDTA 0.05% (Gibco). Cells were either passaged at a 1:3 ratio

in fresh RPMI 10% FBS for cell line maintenance, or diluted in phenol-red-free RPMI medium (Gibco) 5% FBS for microscopy experiments.

Bacterial culture

The UPEC CFT073 strain was originally isolated from a patient with bacteraemia of urinary tract origin (Mobley et al., 1990) and procured from ATCC. CFT073 wild-type and mutant strains were inoculated from frozen stocks in LB Miller medium (Difco) and cultured overnight at 37°C without shaking to induce type 1 pili expression for microscopy experiments (Snyder et al., 2004), or with shaking at 170 rpm for molecular cloning experiments. When required, LB was supplemented with 100 µg/mL ampicillin (Sigma) or 50 µg/mL kanamycin (Sigma).

Construction of the CFT073 Δ fliC sfGFP parental strain

The *fliC* locus (between nucleotides 2,151,497 and 2,153,284) was deleted using the λ Red recombineering system (Datsenko and Wanner, 2000). Briefly, CFT073 was first transformed with plasmid pKD46 to express the λ Red recombinase, then with the kan^R resistance cassette amplified from plasmid pKD4 using primers fliC_KO_F and fliC_KO_R. Successful chromosomal recombination was confirmed by PCR using primers fliC_F and fliC_R, and the kan^R resistance cassette was removed using plasmid pCP20 encoding the FLP recombinase. Loss of swimming motility was assessed by soft-agar assay, as previously described (Lane et al., 2005).

The sfGFP sequence was introduced under control of a strong $P_{\sigma 70}$ promoter at the chromosomal att_{HK022} site (between nucleotides 1,090,927 and 1,090,928) using a recently described method (Eshaghi et al., 2016). Briefly, the kan^R-P_{RhaB}-*relE* toxin cassette was amplified from plasmid pSLC217 using primers P4 and P5 and integrated into the genome of CFT073 Δ*fliC* using λ Red recombineering. Primers P6 and P7 were then used to amplify the sfGFP-containing fragment from plasmid pSLC293, and these PCR amplicons were used to replace the kan^R-P_{RhaB}-*relE* toxin cassette by λ Red recombineering with negative selection on M9 agar (Sigma) supplemented with 0.2% L-rhamnose (Sigma). Successful recombination at each step was confirmed by PCR using primers attHK_F and attHK_R. The same method was used to introduce the sfGFP sequence in the wild-type ($fliC^+$) CFT073 background.

Construction of the transposon insertion library

Tn5 transposon insertion mutants were generated in the CFT073 Δ*fliC* sfGFP parental strain using the EZ-Tn5 transposome kit (Epicentre). Briefly, bacteria were electroporated with transposome complexes and allowed to recover in SOC broth for 1h at 37°C / 170 rpm prior to plating on LB agar supplemented with 50 µg/mL kanamycin and incubation overnight at 37°C. A total of 17,600 mutants was obtained, from which 8,184 were picked, grown overnight in LB kanamycin 50 µg/mL, added with 15% glycerol (Fisher Chemical) and archived in 96-well plates.

Spinfection of bladder epithelial cells with UPEC

CellCarrier™-96 Ultra microplates (Perkin-Elmer) were plasma-activated, coated with an ice-cold solution of 50 µg/mL bovine dermis native collagen (AteloCell) in PBS (Gibco), and incubated for 3h at 37°C for the collagen to polymerize. Wells were washed twice with PBS to remove unbound collagen, seeded with 5637 epithelial cells in phenol-red-free RPMI 5% FBS at a density of 50,000 cells per well, and incubated overnight at 37°C, 5% CO_2 to reach confluency. On the day of the experiment, RPMI was removed from the plates and wells were rinsed once with PBS. Overnight UPEC cultures in 96-well plates were diluted 1:10 in phenol-red-free RPMI 5% FBS and added to the epithelial cells at a multiplicity-of-infection (MOI) of 200:1 using a Liquidator 96 (Mettler-Toledo). Plates were spun down at 600 g for 5 minutes and incubated for 20 minutes at 37°C, 5% CO_2. Wells were then washed twice with PBS to remove non-adherent bacteria and phenol-red free RPMI 5% FBS was added back.

Immunostaining of bladder epithelial cells

Confluent 5637 bladder epithelial cells in 96-well plates were fixed with 4% paraformaldehyde (PFA) for 30 minutes. Fixed cells were washed three times with PBS, permeabilized with 0.15% Triton X-100 for 15 minutes, washed three times with PBS, and blocked with antibody incubation buffer (PBS supplemented with 1% BSA and 0.01% Triton X-100) for 1 hour. Cells were then incubated with primary antibodies (rabbit monoclonal Alexa Fluor® 647 anti-cytokeratin 8 antibody from Abcam, or mouse monoclonal anti-uroplakin IIIa antibody from Santa Cruz) at a 1:100 dilution in antibody incubation buffer overnight at 4°C, and washed three times with PBS. For uroplakin staining, cells were subsequently incubated with secondary antibodies (donkey anti-mouse Alexa Fluor® 647 highly cross-adsorbed IgG from Invitrogen) at a concentration of 2 µg/mL in antibody incubation buffer for 1 hour at room temperature, and washed three times with PBS. Cell nuclei were stained with a 5 µg/mL DAPI (Invitrogen) solution in PBS for 30 minutes, followed by three additional washes with PBS. Cells were imaged with a 63X oil objective on a Leica SP8 confocal microscope, and images were deconvolved using SVI Huygens (Quality, 0.05; Iterations, 40).

High-content imaging of bladder epithelial cells infected with UPEC

Wells containing infected 5637 bladder cells were imaged in 9 fields of view using a high-throughput Operetta CLS microscope (Perkin-Elmer) on the phase-contrast and green fluorescence channels with a 20X air objective (NA = 0.40). The microplate was maintained at 37°C, 5% CO_2 during imaging. Image analysis was performed using the integrated Harmony® high-content analysis software (Perkin-Elmer). Briefly, the mean GFP fluorescence was displayed for each field of view and the average and standard deviation for the 9 fields of view were calculated for each well. For wells where the coefficient of variation (CV) exceeded 10%, images were manually inspected and fields of view with fluorescence artefacts removed from the analysis.

Screening for UPEC mutants with altered adhesion: 1st step

In the first screening step, 96-well plates were arranged with 93 transposon insertion mutants, the Δ*fliC* parental strain, the Δ*fliC dsbA*-Tn low-adhesion strain, and one blank well containing LB medium only. After overnight culture, they were used to infect 5637 bladder epithelial cells following the aforementioned procedure. OD_{600} was also recorded for each well and mutants that did not grow were removed from the analysis. After spinfection and imaging, the average and standard deviation of GFP fluorescence on a particular plate were calculated based on the individual fluorescence values for each well, and mutants with values more than 1.5 standard deviations from the average were selected for retesting. We always made sure that the value for the Δ*fliC* parental strain was less than 1.5 standard deviations from the average, and that the value for the Δ*fliC dsbA*-Tn low-adhesion strain was more than 2 standard deviations from the average, otherwise the experiment was repeated for that particular plate. We also visually controlled the integrity of the epithelial cell layer in each well by phase-contrast microscopy.

Screening for UPEC mutants with altered adhesion: 2nd step

In the second screening step, 96-well plates were arranged with 3 wells of each candidate mutant and 30 wells containing the Δ*fliC* parental strain. After overnight culture, they were used to infect 5637 bladder epithelial cells following the aforementioned procedure. After spinfection and imaging, the average and standard deviation of GFP fluorescence were calculated for the 30 replicates of the parental strain, and mutants with values more than 2 standard deviations from the average were selected for retesting.

Screening for UPEC mutants with altered adhesion: 3rd step

In the third screening step, candidate mutants were cultured overnight in individual flasks along with the Δ*fliC* parental strain. All cultures were adjusted to the same final OD_{600} value in pre-warmed phenol-red-free RPMI 5% FBS, so that this would correspond to a 1:10 dilution for the mutant with the lowest overnight OD_{600}. 96-well plates were arranged with 6 wells of each mutant and 6 wells containing the Δ*fliC* parental strain. The rest of the procedure was conducted as described above. For each mutant, the distribution of GFP fluorescence values after spinfection was compared to the distribution for the Δ*fliC* parental strain using Welch's t-test and strains with $P < 0.05$ were selected for further analysis.

Identification of transposon insertion sites by RATE (rapid amplification of transposon ends) PCR

Tn5 insertion sites were identified using a single-primer PCR protocol adapted from Ducey et al. Briefly, candidate mutants were streaked on LB agar supplemented with 50 µg/mL kanamycin. A single colony was boiled for 10 minutes in 50 µL water and 1 µL was used as template in a standard 50-µL PCR reaction with primer R6K_inv1 using a double amount of Platinum® *Taq* High Fidelity DNA Polymerase (Invitrogen). The first 30 cycles of the PCR reaction were done at 55°C with a 60-sec extension time; the next 30 cycles were done at 30°C with a similar extension time; and the last 30 cycles were performed at 55°C with a 2-minute extension time. PCR amplicons were then sent for sequencing using the nested R6K_RP1 primer, and the sequence was aligned to the CFT073 chromosome.

Assignment of P pili transposon insertions to the pap1 or pap2 operon

To determine whether a transposon insertion occurred within the *pap1* or *pap2* operon, we performed a dual set of standard 25-µL Q5® PCR reactions (New England Biolabs) using a first primer specific to the transposon sequence, and a second primer specific to the DNA sequence flanking either of the two operons. Primer pairs were chosen based on the position and orientation of each transposon insertion, as indicated in Supplementary Table S4. PCR amplicons were analysed on 1% agarose gels stained with SYBR® Safe DNA Gel Stain (Invitrogen), and identification of the gene disrupted was based on the brightest amplicon band.

Construction of unmarked UPEC deletion strains

The *fimH* locus (between nucleotides 5,143,529 and 5,144,440), *fim* operon (between nucleotides 5,135,689 and 5,144,440), *foc* operon (between nucleotides 1,188,213 and 1,194,827) and *pap* operons (*pap1* operon between nucleotides 3,429,593 and 3,437,564; *pap2* operon between nucleotides 4,940,831 and 4,948,799) were deleted from CFT073 sfGFP and CFT073 Δ*fliC* sfGFP using the λ Red recombineering system as described above. The kan^R resistance cassette was amplified from plasmid pKD4 using primer pairs fimH_KO_F + fimH_KO_R, fimB_KO_F + fimH_KO_R, focA_KO_F + focH_KO_R, and papA_KO_F + papG_KO_R respectively. For deletion of the *pap* operons, we used the same primer pair for integration of the kan^R resistance cassette in place of either operon and then identified the disrupted operon using specific primer pairs. Successful chromosomal recombination was confirmed by PCR using primer pairs fimH_F + fimH_R for Δ*fimH*, fimB_F + fimH_R for Δ*fim*, focA_F + focH_R for Δ*foc*, papI_F + papG_R for Δ*pap1*, and papI2_F + papG2_R for Δ*pap2*. The double *pap* deletion mutants were obtained by successively deleting the *pap1* and *pap2* operons from CFT073 sfGFP and CFT073 Δ*fliC* sfGFP. Adhesion phenotypes of all mutants were assessed using the same method as in the third step of the screen. To be able to pool data coming from different experiments, results were normalized to the Δ*fliC* parental strain in each experiment.

Quantitative real-time PCR (qRT-PCR)

CFT073 mutant strains cultured overnight in static conditions were pelleted and RNA was extracted using the High Pure RNA Isolation kit (Roche) according to the manufacturer's instructions. RNA samples were DNAse-treated using the TURBO DNA-*free*™ kit (Invitrogen), and cDNA was obtained using the SuperScript™ IV reverse transcriptase with random hexamers (Invitrogen). qRT-PCR reactions were set up using the SYBR® Green PCR Master Mix (Applied Biosystems) with 2.5 µM primers and 30 ng cDNA. Reactions were run on an ABI PRISM7900HT Sequence Detection System (Applied Biosystems). For each gene and each experiment, relative expression levels were calculated by normalizing to the expression level of the housekeeping gene *gapA* and to the expression level in the Δ*fliC* parental strain.

Biotinylation of surface-exposed proteins and protein affinity purification

The bacterial surface proteome was isolated as described by Monteiro et al. Briefly, CFT073 mutant strains cultured overnight in static conditions were pelleted, washed twice with PBS, and incubated for 30 minutes in PBS supplemented with 1% (m/m) sulfo-NHS-SS-biotin (Thermo Scientific Pierce™) under gentle agitation at room temperature. Excess of the biotinylation reagent was quenched by three washes with a 500 mM glycine (AppliChem) solution in PBS, and bacteria were resuspended in PBS supplemented with 1% (v/v) Triton X-100 and Protease Inhibitor Cocktail (Roche). Cell lysis was performed using FastPrep (MP Biomedicals) with two steps of 20 sec at 6 m/s, and cell debris were pelleted by centrifugation at 20,000 g for 30 minutes. Biotinylated proteins in the supernatant were affinity-purified using High Capacity NeutrAvidin™ Agarose (Thermo Scientific Pierce™) according to the manufacturer's instructions. Briefly, agarose slurry was packed into 2 mL Centrifuge Columns (Thermo Scientific Pierce™), washed with 3 column volumes of PBS, and incubated with protein samples for 60 minutes at 4°C under gentle rotation. Unlabelled proteins were washed away with 5 column volumes of PBS, and biotinylated proteins were eluted with DTT-modified Laemmli buffer (2% SDS, 20% glycerol, 62.5 mM Tris-HCl, 50 mM DTT, 5% ß-mercaptoethanol). The protein concentration in eluted samples was assessed using the Pierce™ 660nm Protein Assay (Thermo Scientific Pierce™) according to the manufacturer's recommendations for samples eluted in Laemmli buffer. To assess the efficiency of the surface biotinylation and affinity-purification steps (Supplementary Figure S8A), CFT073 Δ*fliC* sfGFP protein samples were prepared as described above, except that lysis was performed with 2% SDS (Sigma). Samples before affinity-purification (total cell extracts) were then directly analysed by mass spectrometry along with affinity-purified samples (surfaceomes).

Protein sample preparation

Mass spectrometry-based proteomics-related experiments were performed by the Proteomics Core Facility at EPFL. Protein samples (10 µg per dataset) were loaded on an SDS-PAGE gel and allowed for a short migration. The gel pieces containing the concentrated proteins were excised, washed twice with 50% ethanol in 50 mM ammonium bicarbonate (AB, Sigma) for 20 minutes, and dried by vacuum centrifugation. Proteins were reduced with 10 mM dithioerythritol (Merck-Millipore) for 1 hour at 56°C followed by washing/drying. Reduced proteins were alkylated with 55 mM iodoacetamide (Sigma) for 45 minutes at 37°C in the dark followed by washing/drying. Alkylated proteins were digested overnight at 37°C using mass spectrometry grade Trypsin Gold (Promega) at a concentration of 12.5 ng/µL in 50 mM AB supplemented with 10 mM $CaCl_2$. Resulting peptides were extracted in 70% ethanol, 5% formic acid (FA, Merck-Millipore) twice for 20 minutes, dried by vacuum centrifugation and stored at -20°C until further analysis.

Mass spectrometry analysis

Peptides were desalted on C_{18} StageTips (Rappsilber et al., 2007) and dried by vacuum centrifugation prior to LC-MS/MS injections. Samples were resuspended in 2% acetonitrile (Biosolve), 0.1% FA and nano-flow separations were performed on a Dionex UltiMate™ 3000 RSLCnano UPLC system (Thermo Scientific™) on-line connected with an Orbitrap Exploris™ 480 mass spectrometer (Thermo Scientific™). A

capillary precolumn (Acclaim™ PepMap™ C_{18}, 3 µm-100Å, 2 cm x 75 µm i.d.) was used for sample trapping and cleaning. A 50cm long capillary column (75 µm i.d., in-house packed using ReproSil-Pur C_{18}-AQ 1.9 µm silica beads, Dr. Maisch) was then used for analytical separations at 250 nL/min over 150-minute biphasic gradients. Acquisitions were performed through Top Speed Data-Dependent acquisition mode using a cycle time of 2 seconds. First MS scans were acquired with a resolution of 60'000 (at 200 m/z) and the most intense parent ions were selected and fragmented by High energy Collision Dissociation (HCD) with a Normalized Collision Energy (NCE) of 30% using an isolation window of 2 m/z. Fragmented ions were acquired with a resolution of 15'000 (at 200 m/z) and selected ions were then excluded for the following 20 seconds.

Bioinformatic analysis

Raw data were processed using MaxQuant 1.6.10.43 (Cox and Mann, 2008) against the *Escherichia coli* CFT073 Uniprot database (5336 entries, last modification 210307) Carbamidomethylation was set as fixed modification, whereas oxidation (M), phosphorylation (S, T, Y), acetylation (Protein N-term), CAMthiopropanoyl (K and Protein N-term) and glutamine to pyroglutamate were considered as variable modifications. A maximum of two missed cleavages were allowed and "Match between runs" option was enabled. A minimum of two peptides was required for protein identification and the false discovery rate (FDR) cutoff was set to 0.01 for both peptides and proteins. Label-free quantification and normalisation was performed by MaxQuant using the MaxLFQ algorithm, with the standard settings (Cox et al., 2014).

The statistical analysis was performed using Perseus 1.6.12.0 (Tyanova et al., 2016) from the MaxQuant tool suite. Reverse proteins, potential contaminants and proteins only identified by sites were filtered out. Protein groups containing at least three valid values in at least one group were conserved for further analysis. Empty values were imputed with random numbers from a normal distribution (width: 0.3, down shift: 1.8 sd). A two-sample t-test with permutation-based FDR statistics (250 permutations, FDR = 0.01, S0 = 0.5) was performed to determine significant differentially abundant candidates. Further graphical displays were performed using homemade programs written in R (https://www.R-project.org/).

Scanning electron microscopy (SEM) sample preparation

5637 bladder epithelial cells spinfected with UPEC in μ-dishes (Ibidi) or CFT073 mutant strains left to adhere for 20 minutes on poly-L-lysine-coated coverslips were fixed for 30 minutes with 1.25% glutaraldehyde in PBS 0.1M pH 7.4. Samples were post-fixed for 30 minutes with 0.2% osmium tetroxide in 0.1 M cacodylate buffer followed by washing with distilled water. Next, samples were dehydrated in graded ethanol series and dried in an automated critical point dryer (Leica Microsystems). Finally, samples were attached to an adhesive conductive surface followed by coating with 3–4 nm of gold/palladium (Quorum Technologies). Images of the samples were acquired using a field emission scanning electron microscope (Zeiss NTS).

Automated quantification of single-cell piliation using Ilastik

The Ilastik software (https://www.ilastik.org) was trained by manually annotating background, pili and bacterial body on four SEM images of the Δ*fliC* parental strain. After applying the trained software on an SEM image, the channel corresponding to the bacterial body was further processed using Fiji: a threshold was applied to keep only pixels with intensity values from 0.30 to 1, holes were filled, and particles were analysed to keep only circular particles with an area above 250,000 pixels. The channel corresponding to the pili was then subtracted with the processed bacterial body, a threshold was applied to keep only pixels with intensity values between 0.55 and 1, and particles were analysed to keep non-circular particles (circularity = 0.00-0.20) with an area above 100 pixels, resulting in the processed pili image (see also Supplementary Figure S9). Single-cell piliation was calculated for each image by simply dividing the area of the pili by the area of the bacterial body. To be able to pool data coming from different experiments, results were normalized to the Δ*fliC* parental strain in each experiment.

Gentamicin protection assay to assess bacterial invasion

Invasion assays were performed essentially as described by Martinez et al. Briefly, confluent 5637 bladder epithelial cells in two sets of triplicate wells were spinfected with UPEC in RPMI 5% FBS at a MOI of 50:1. Plates were incubated for 20 minutes at 37°C, 5% CO_2 and washed twice with PBS to remove non-adherent bacteria. One set of triplicate wells was lysed by the addition of trypsin-EDTA and Triton X-100, both at final concentration of 0.05%, and bacteria in these lysates were titered on LB agar plates, representing the adherent UPEC fraction. The second set of triplicate wells was added back with RPMI 5% FBS, incubated for 2 hours, washed twice with PBS, and incubated for another 2 hours in RPMI 5% FBS containing 100 µg/mL gentamicin (Gibco) to kill extracellular bacteria. Wells were then washed twice with PBS, lysed and titered, representing the invasive UPEC fraction. Invasion frequencies were calculated by dividing the number of bacteria in the invasive fraction by the number of bacteria in the adhesive fraction.

References

1. Agata, N. *et al.* Serological response to P-fimbriae of *Escherichia coli* in patients with urinary tract infections. Eur J Clin Microbiol Infect Dis **8**(**2**), 156–159 (1989).
2. Anderson, G. G. *et al.* Intracellular Bacterial Biofilm-Like Pods in Urinary Tract Infections. Science **301**, 105–107 (2003).
3. Barber, A. E., Norton, J. P., Wiles, T. J. & Mulvey, M. A. Strengths and Limitations of Model Systems for the Study of Urinary Tract Infections and Related Pathologies. Microbiol. Mol. Biol. Rev. **80**, 351–367 (2016).
4. Bates, J. M. *et al.* Tamm-Horsfall protein knockout mice are more prone to urinary tract infection. Kidney International **65**, 791–797 (2004).
5. Beloin, C. *et al.* The Transcriptional Antiterminator RfaH Represses Biofilm Formation in *Escherichia coli*. J Bacteriol **188**, 1316–1331 (2006).
6. Bien, J., Sokolova, O. & Bozko, P. Role of Uropathogenic *Escherichia coli* Virulence Factors in Development of Urinary Tract Infection and Kidney Damage. International Journal of Nephrology

2012, 1–15 (2012).

7. Blango, M. G. & Mulvey, M. A. Persistence of Uropathogenic *Escherichia coli* in the Face of Multiple Antibiotics. Antimicrob Agents Chemother **54**, 1855–1863 (2010).
8. Conover, M. S. *et al.* Inflammation-Induced Adhesin-Receptor Interaction Provides a Fitness Advantage to Uropathogenic *E. coli* during Chronic Infection. Cell Host & Microbe **20**, 482–492 (2016).
9. Cox, J. *et al*. Accurate proteome-wide label-free quantification by delayed normalization and maximal peptide ratio extraction, termed MaxLFQ. Mol Cell Proteomics. **13**(**9**), 2513–26 (2014).
10. Cox, J. & Mann, M. MaxQuant enables high peptide identification rates, individualized p.p.b.-range mass accuracies and proteome-wide protein quantification. Nat Biotechnol **26**, 1367–1372 (2008).
11. Datsenko, K. A. & Wanner, B. L. One-step inactivation of chromosomal genes in *Escherichia coli* K-12 using PCR products. *Proceedings of the National Academy of Sciences* **97**, 6640–6645 (2000).
12. de Ree, J. M. & van den Bosch, J. F. Serological response to the P fimbriae of uropathogenic *Escherichia coli* in pyelonephritis. Infect Immun **55**, 2204–2207 (1987).
13. Dodson, K. W. *et al.* Structural Basis of the Interaction of the Pyelonephritic *E. coli* Adhesin to Its Human Kidney Receptor. Cell **105**, 733–743 (2001).
14. Ducey, T. F. & Dyer, D. W. Rapid identification of EZ::TN transposon insertion sites in the genome of *Neisseria gonorrhoeae*. Epicentre Forum **9**, 6–7 (2002).
15. Duraiswamy, S. *et al.* Purification of Intracellular Bacterial Communities during Experimental Urinary Tract Infection Reveals an Abundant and Viable Bacterial Reservoir. Infection and Immunity **86**, 15 (2018).
16. Ejrnaes, K. *et al.* Pulsed-Field Gel Electrophoresis Typing of *Escherichia coli* Strains from Samples Collected before and after Pivmecillinam or Placebo Treatment of Uncomplicated Community-Acquired Urinary Tract Infection in Women. J Clin Microbiol **44**, 1776–1781 (2006).
17. Eshaghi, M., Mehershahi, K. S. & Chen, S. L. Brighter Fluorescent Derivatives of UTI89 Utilizing a Monomeric vGFP. *Pathogens* **5**, (2016).
18. Flores-Mireles, A. L., Walker, J. N., Caparon, M. & Hultgren, S. J. Urinary tract infections: epidemiology, mechanisms of infection and treatment options. Nat Rev Microbiol **13**, 269–284 (2015).
19. Foxman, B. Epidemiology of urinary tract infections: incidence, morbidity, and economic costs. The American Journal of Medicine **113**, 5–13 (2002).
20. Foxman, B. The epidemiology of urinary tract infection. Nat Rev Urol **7**, 653–660 (2010).
21. Foxman, B. Urinary Tract Infection Syndromes. Infectious Disease Clinics of North America **28**, 1–13 (2014).
22. Foxman, B., Barlow, R., D'Arcy, H., Gillespie, B. & Sobel, J. D. Urinary Tract Infection: Self-Reported Incidence and Associated Costs. **10**, 7 (2000).
23. Greene, S. E., Hibbing, M. E., Janetka, J., Chen, S. L. & Hultgren, S. J. Human Urine Decreases Function and Expression of Type 1 Pili in Uropathogenic Escherichia coli. *mBio* **6**, (2015).

24. Hagan, E. C., Lloyd, A. L., Rasko, D. A., Faerber, G. J. & Mobley, H. L. T. *Escherichia coli* Global Gene Expression in Urine from Women with Urinary Tract Infection. PLoS Pathog **6**, e1001187 (2010).
25. Hannan, T. J. *et al.* Host-pathogen checkpoints and population bottlenecks in persistent and intracellular uropathogenic *Escherichia coli* bladder infection. FEMS Microbiol Rev **36**, 616–648 (2012).
26. Holden, N. J. & Gally, D. L. Switches, cross-talk and memory in *Escherichia coli* adherence. Journal of Medical Microbiology **53**, 585–593 (2004).
27. Hung, C.-S. *et al.* Structural basis of tropism of *Escherichia coli* to the bladder during urinary tract infection: FimH mannose-binding pocket. Molecular Microbiology **44**, 903–915 (2002).
28. Iosifidis, G. & Duggin, I. G. Distinct Morphological Fates of Uropathogenic *Escherichia coli* Intracellular Bacterial Communities: Dependency on Urine Composition and pH. Infect Immun **88**, (2020).
29. Jacob-Dubuisson, F. *et al.* PapD chaperone function in pilus biogenesis depends on oxidant and chaperone-like activities of DsbA. *Proceedings of the National Academy of Sciences* **91**, 11552–11556 (1994).
30. Johnson, J. R., Owens, K., Gajewski, A. & Kuskowski, M. A. Bacterial Characteristics in Relation to Clinical Source of *Escherichia coli* Isolates from Women with Acute Cystitis or Pyelonephritis and Uninfected Women. J Clin Microbiol **43**, 6064–6072 (2005).
31. Justice, S. S. *et al.* Differentiation and developmental pathways of uropathogenic *Escherichia coli* in urinary tract pathogenesis. *Proceedings of the National Academy of Sciences* **101**, 1333–1338 (2004).
32. Kalas, V. *et al.* Evolutionary fine-tuning of conformational ensembles in FimH during host-pathogen interactions. Sci. Adv. **3**, e1601944 (2017).
33. Katchman, E. A. *et al.* Three-day vs longer duration of antibiotic treatment for cystitis in women: Systematic review and meta-analysis. The American Journal of Medicine **118**, 1196–1207 (2005).
34. Klein, R. D. & Hultgren, S. J. Urinary tract infections: microbial pathogenesis, host–pathogen interactions and new treatment strategies. Nat Rev Microbiol **18**, 211–226 (2020).
35. Kline, K. A., Fälker, S., Dahlberg, S., Normark, S. & Henriques-Normark, B. Bacterial Adhesins in Host-Microbe Interactions. Cell Host & Microbe **5**, 580–592 (2009).
36. Lacerda Mariano, L. & Ingersoll, M. A. The immune response to infection in the bladder. Nat Rev Urol **17**, 439–458 (2020).
37. Lane, M. C. Role of P-fimbrial-mediated adherence in pyelonephritis and persistence of uropathogenic *Escherichia coli* (UPEC) in the mammalian kidney. Kidney International **7** (2007).
38. Lane, M. C. *et al.* Role of motility in the colonization of uropathogenic *Escherichia coli* in the urinary tract. Infect. Immun. **73**, 7644–7656 (2005).
39. Lewis, A. J., Richards, A. C. & Mulvey, M. A. Invasion of Host Cells and Tissues by Uropathogenic Bacteria. Microbiol Spectr **4** (2016).

40. Lillington, J. Biogenesis and adhesion of type 1 and P pili. Biochimica et Biophysica Acta **11** (2014).
41. Lloyd, A. L., Rasko, D. A. & Mobley, H. L. T. Defining Genomic Islands and Uropathogen-Specific Genes in Uropathogenic *Escherichia coli*. J Bacteriol **189**, 3532–3546 (2007).
42. Martinez, J. J. Type 1 pilus-mediated bacterial invasion of bladder epithelial cells. The EMBO Journal **19**, 2803–2812 (2000).
43. Mobley, H. L. *et al.* Pyelonephritogenic *Escherichia coli* and killing of cultured human renal proximal tubular epithelial cells: role of hemolysin in some strains. Infection and Immunity **58**, 1281–1289 (1990).
44. Monteiro, R. *et al.* Differential biotin labelling of the cell envelope proteins in lipopolysaccharidic diderm bacteria: Exploring the proteosurfaceome of *Escherichia coli* using sulfo-NHS-SS-biotin and sulfo-NHS-PEG4-bismannose-SS-biotin. Journal of Proteomics **181**, 16–23 (2018).
45. Mulvey, M. A. *et al.* Induction and Evasion of Host Defenses by Type 1-Piliated Uropathogenic *Escherichia coli*. Science **282**, 1494–1497 (1998).
46. Murray, B. O. *et al.* Recurrent Urinary Tract Infection: A Mystery in Search of Better Model Systems. Front. Cell. Infect. Microbiol. **11**, 691210 (2021).
47. Mysorekar, I. U. & Hultgren, S. J. Mechanisms of uropathogenic *Escherichia coli* persistence and eradication from the urinary tract. *Proceedings of the National Academy of Sciences* **103**, 14170–14175 (2006).
48. Nicolle, L. E. Uncomplicated Urinary Tract Infection in Adults Including Uncomplicated Pyelonephritis. Urologic Clinics of North America **35**, 1–12 (2008).
49. Pak, J., Pu, Y., Zhang, Z.-T., Hasty, D. L. & Wu, X.-R. Tamm-Horsfall Protein Binds to Type 1 Fimbriated *Escherichia coli* and Prevents E. *coli* from Binding to Uroplakin Ia and Ib Receptors. *Journal of Biological Chemistry* **276**, 9924–9930 (2001).
50. Pizarro-Cerdá, J. & Cossart, P. Bacterial Adhesion and Entry into Host Cells. Cell **124**, 715–727 (2006).
51. Rappsilber, J., Mann, M. & Ishihama, Y. Protocol for micro-purification, enrichment, pre-fractionation and storage of peptides for proteomics using StageTips. Nat Protoc **2**, 1896–1906 (2007).
52. Roberts, J. A. *et al.* The Gal(al-4)Gal-specific tip adhesin of *Escherichia coli* P-fimbriae is needed for pyelonephritis to occur in the normal urinary tract. *Proc. Natl. Acad. Sci. USA* **5** (1994).
53. Sarshar, M. *et al.* FimH and Anti-Adhesive Therapeutics: A Disarming Strategy Against Uropathogens. Antibiotics **9**, 397 (2020).
54. Schembri, M. A., Dalsgaard, D. & Klemm, P. Capsule Shields the Function of Short Bacterial Adhesins. J Bacteriol **186**, 1249–1257 (2004).
55. Scholes, D. *et al.* Risk Factors Associated with Acute Pyelonephritis in Healthy Women. Ann Intern Med **142**, 20–27 (2005)
56. Schwartz, D. J., Chen, S. L., Hultgren, S. J. & Seed, P. C. Population Dynamics and Niche Distribution of Uropathogenic *Escherichia coli* during Acute and Chronic Urinary Tract Infection. Infect Immun **79**, 4250–4259 (2011).

57. Seminerio, J. L., Aggarwal, G. & Sweetser, S. 26-Year-Old Man With Recurrent Urinary Tract Infections. *Mayo Clinic Proceedings* **86**, 557–560 (2011).
58. Sharma, K. *et al.* Early invasion of the bladder wall by solitary bacteria protects UPEC from antibiotics and neutrophil swarms in an organoid model. Cell Reports **36**, 109351 (2021a).
59. Sharma, K. *et al.* Dynamic persistence of UPEC intracellular bacterial communities in a human bladder-chip model of urinary tract infection. eLife **10**, e66481 (2021b).
60. Simmering, J. E., Tang, F., Cavanaugh, J. E., Polgreen, L. A. & Polgreen, P. M. The Increase in Hospitalizations for Urinary Tract Infections and the Associated Costs in the United States, 1998–2011. Open Forum Infectious Diseases **4** (2017).
61. Snyder, J. A. *et al.* Transcriptome of Uropathogenic *Escherichia coli* during Urinary Tract Infection. Infect Immun **72**, 9 (2004).
62. Spaulding, C. N. *et al.* Selective depletion of uropathogenic *E. coli* from the gut by a FimH antagonist. Nature **546**, 528–532 (2017).
63. Spurbeck, R. R. *et al.* Fimbrial Profiles Predict Virulence of Uropathogenic *Escherichia coli* Strains: Contribution of Ygi and Yad Fimbriae. Infect. Immun. **79**, 4753–4763 (2011).
64. Stracy, M. *et al.* Minimizing treatment-induced emergence of antibiotic resistance in bacterial infections. Science **375**, 889–894 (2022).
65. Subashchandrabose, S. *et al.* Host-specific induction of *Escherichia coli* fitness genes during human urinary tract infection. Proc Natl Acad Sci USA **111**, 18327–18332 (2014).
66. Terlizzi, M. E., Gribaudo, G. & Maffei, M. E. UroPathogenic *Escherichia coli* (UPEC) Infections: Virulence Factors, Bladder Responses, Antibiotic, and Non-antibiotic Antimicrobial Strategies. Front. Microbiol. **8**, 1566 (2017).
67. Thanassi, D. G., Bliska, J. B. & Christie, P. J. Surface organelles assembled by secretion systems of Gram-negative bacteria: diversity in structure and function. FEMS Microbiol Rev **36**, 1046–1082 (2012).
68. Thumbikat, P. *et al.* Bacteria-Induced Uroplakin Signaling Mediates Bladder Response to Infection. PLoS Pathog **5**, e1000415 (2009).
69. Totsika, M., Beatson, S. A., Holden, N. & Gally, D. L. Regulatory interplay between pap operons in uropathogenic *Escherichia coli*. Mol Microbiol **67**, 996–1011 (2008).
70. Tyanova, S. *et al.* The Perseus computational platform for comprehensive analysis of (prote)omics data. Nat Methods **13**, 731–740 (2016).
71. van der Woude, M. W. & Bäumler, A. J. Phase and Antigenic Variation in Bacteria. Clin Microbiol Rev **17**, 581–611 (2004).
72. Verderosa, A. D. *et al.* A high-throughput cell-based assay pipeline for the preclinical development of bacterial DsbA inhibitors as antivirulence therapeutics. Sci Rep **11**, 1569 (2021).
73. Virkola, R. *et al.* Binding characteristics of *Escherichia coli* adhesins in human urinary bladder. Infect Immun **56**, 2615–2622 (1988).

74. Waksman, G. & Hultgren, S. J. Structural biology of the chaperone–usher pathway of pilus biogenesis. Nat Rev Microbiol **7**, 765–774 (2009).
75. Weiss, G. L. *et al.* Architecture and function of human uromodulin filaments in urinary tract infections. Science **369**, 1005–1010 (2020).
76. Welch, R. A. *et al.* Extensive mosaic structure revealed by the complete genome sequence of uropathogenic *Escherichia coli*. *Proc. Natl. Acad. Sci. U.S.A.* **99**, 17020–17024 (2002).
77. Wiles, T. J., Kulesus, R. R. & Mulvey, M. A. Origins and virulence mechanisms of uropathogenic *Escherichia coli*. Experimental and Molecular Pathology **85**, 11–19 (2008).
78. Wright, K. J., Seed, P. C. & Hultgren, S. J. Development of intracellular bacterial communities of uropathogenic *Escherichia coli* depends on type 1 pili. Cellular Microbiology **9**, 2230–2241 (2007).
79. Wu, X.-R. In vitro binding of type 1-fimbriated *Escherichia coli* to uroplakins Ia and Ib: Relation to urinary tract infections. Cell Biology **6** (1996).
80. Wurpel, D. J., Beatson, S. A., Totsika, M., Petty, N. K. & Schembri, M. A. Chaperone-Usher Fimbriae of *Escherichia coli*. PLoS ONE **8**, e52835 (2013).
81. Wurpel, D. J. *et al.* F9 Fimbriae of Uropathogenic *Escherichia coli* Are Expressed at Low Temperature and Recognise Galβ1-3GlcNAc-Containing Glycans. PLoS ONE **9**, e93177 (2014).
82. Zhou, G. *et al.* Uroplakin Ia is the urothelial receptor for uropathogenic *Escherichia coli*: evidence from in vitro FimH binding. Journal of Cell Science **114**, 4095–4103 (2001).
83. Zilsel, J., Ma, P. H. & Beatty, J. T. Derivation of a mathematical expression useful for the construction of complete genomic libraries. Gene **120**, 89–92 (1992).

Figures

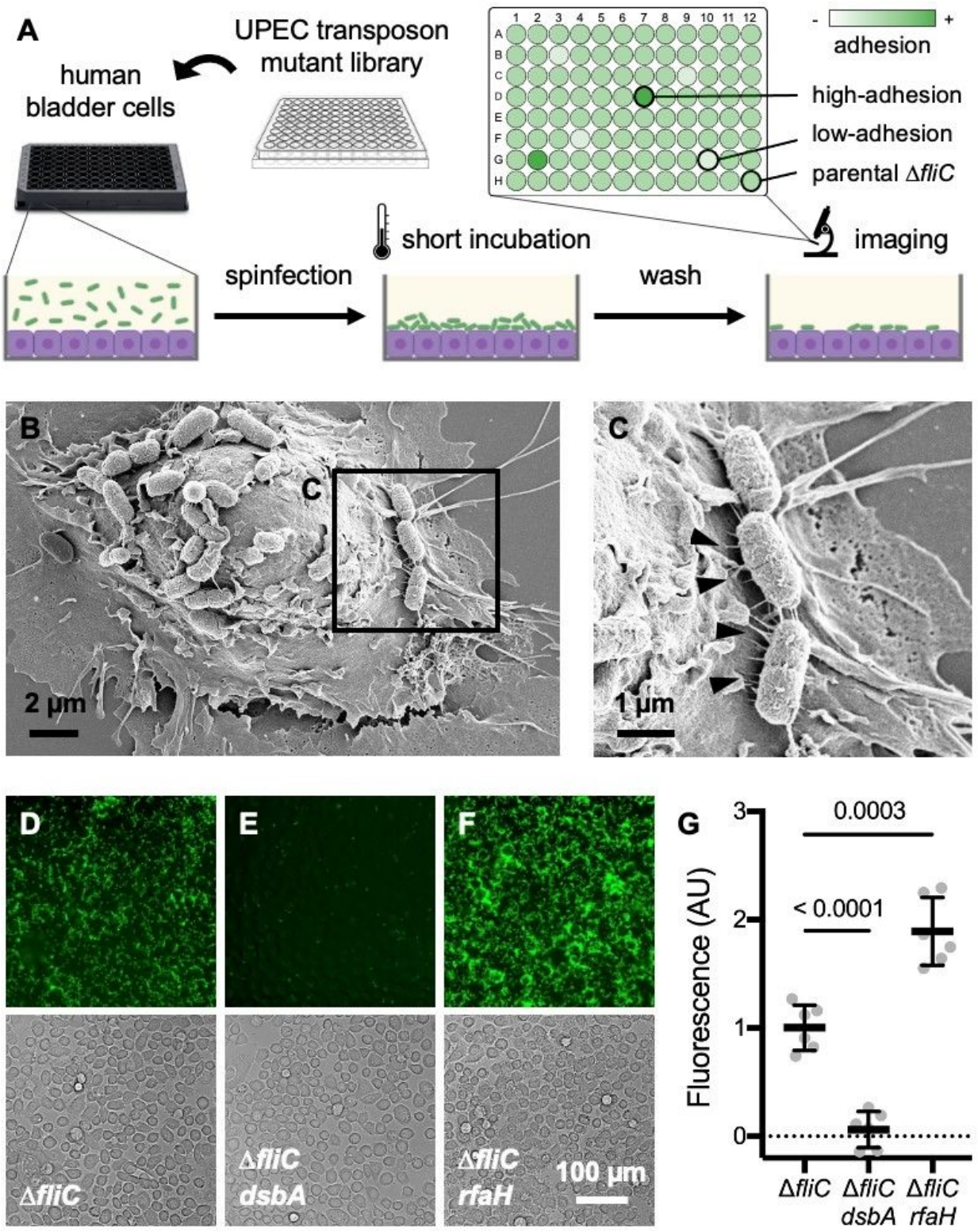

Figure 1

A high-content screening method identifies UPEC mutants with altered adhesion to bladder epithelial cells. (A) Schematic of the high-content screening assay. Confluent 5637 human bladder epithelial cells in 96-well plates were spinfected with UPEC transposon mutants constructed in the parental strain CFT073 Δ*fliC* sfGFP (hereafter referred to as *ΔfliC*). Plates were incubated, washed to remove non-adherent bacteria, and imaged on phase-contrast and green fluorescence channels using a high-throughput

microscope. Quantification of GFP fluorescence served as a proxy for the number of adherent bacteria in each well. A total of 8,184 transposon mutants was screened (see detailed workflow in **Supplementary Figure S2**). **(B)** Scanning electron micrograph showing the interaction between the Δ*fliC* parental strain and bladder epithelial cells. Scale bar: 2 µm. **(C)** Zoom of the boxed area in panel **(B)** showing that bacterial adhesion to bladder cells is mediated by pili, indicated by black arrowheads. Scale bar: 1 µm. **(D-F)** Representative images of bladder epithelial cells spinfected with the Δ*fliC* parental strain **(D)**, Δ*fliC dsbA*-Tnlow-adhesion mutant **(E)**, and Δ*fliC rfaH*-Tn high-adhesion mutant **(F)**, imaged on the green fluorescence channel to quantify adherent bacteria (upper panels) and phase-contrast channel to confirm the integrity of the epithelial cell layer (lower panels). Scale bar: 100 µm for all images. **(G)** Quantification of GFP fluorescence for each strain. n = 6 wells per strain; data were normalized to the Δ*fliC* parental strain; black lines indicate mean and standard deviation; *P*-values were calculated using Welch's t-test.

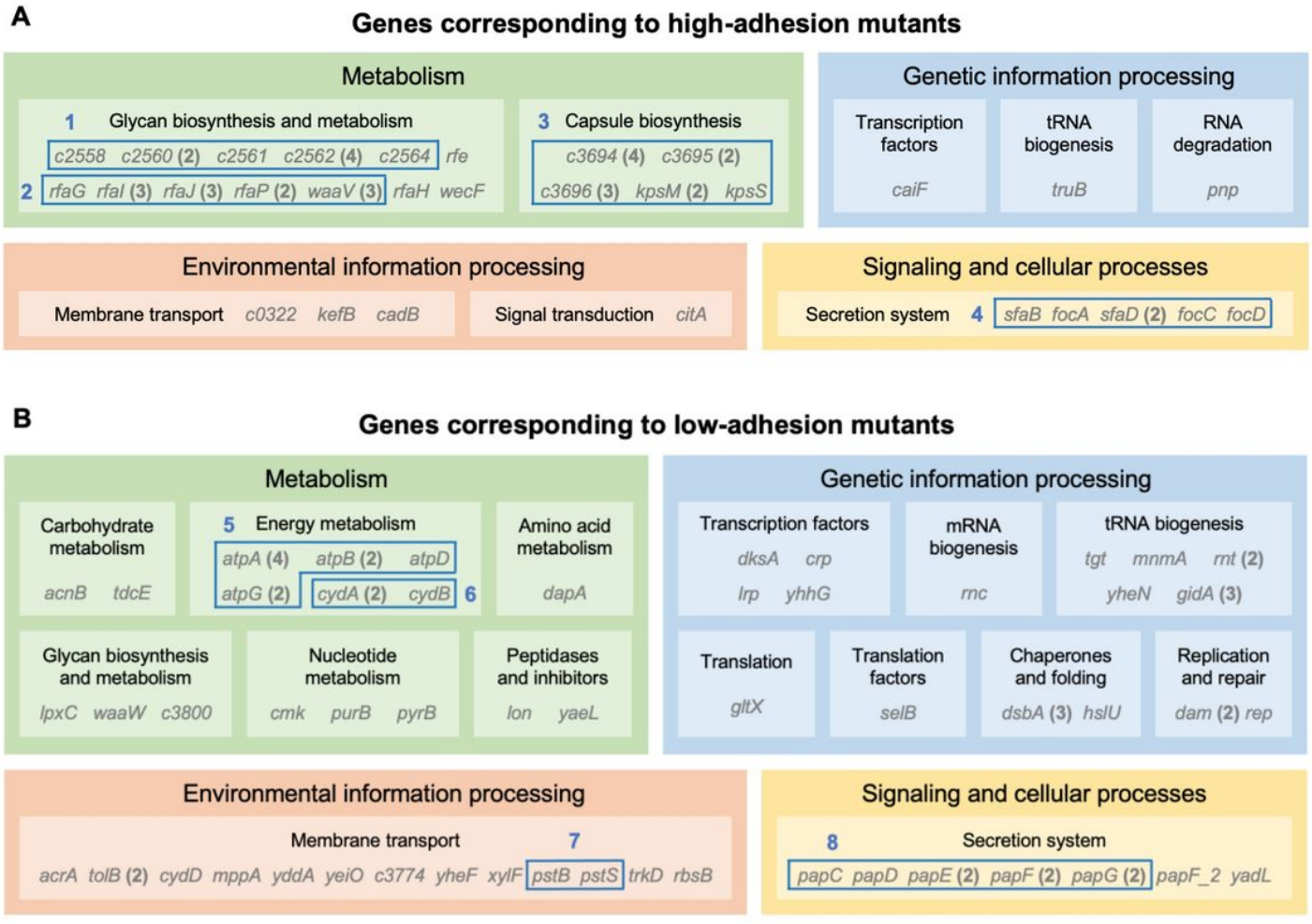

Figure 2

Early adhesion of UPEC to bladder epithelial cells is differentially regulated by multiple genes. Genes disrupted in UPEC transposon mutants with increased **(A)** or decreased **(B)** adhesion to bladder epithelial

cells were grouped according to their KEGG classification. Genes that do not have a KEGG annotation are listed in **Supplementary Table S1**. Numbers in parentheses indicate the number of independent transposon hits obtained in the corresponding genes. Genes that belong to the same operon are framed in blue: **(1)** O-antigen synthesis; **(2)** LPS core synthesis; **(3)** capsule synthesis; **(4)** F1C pili synthesis; **(5)** ATP synthase; **(6)** cytochrome bd; **(7)** Pst system; **(8)** P pili synthesis (*pheV* operon).

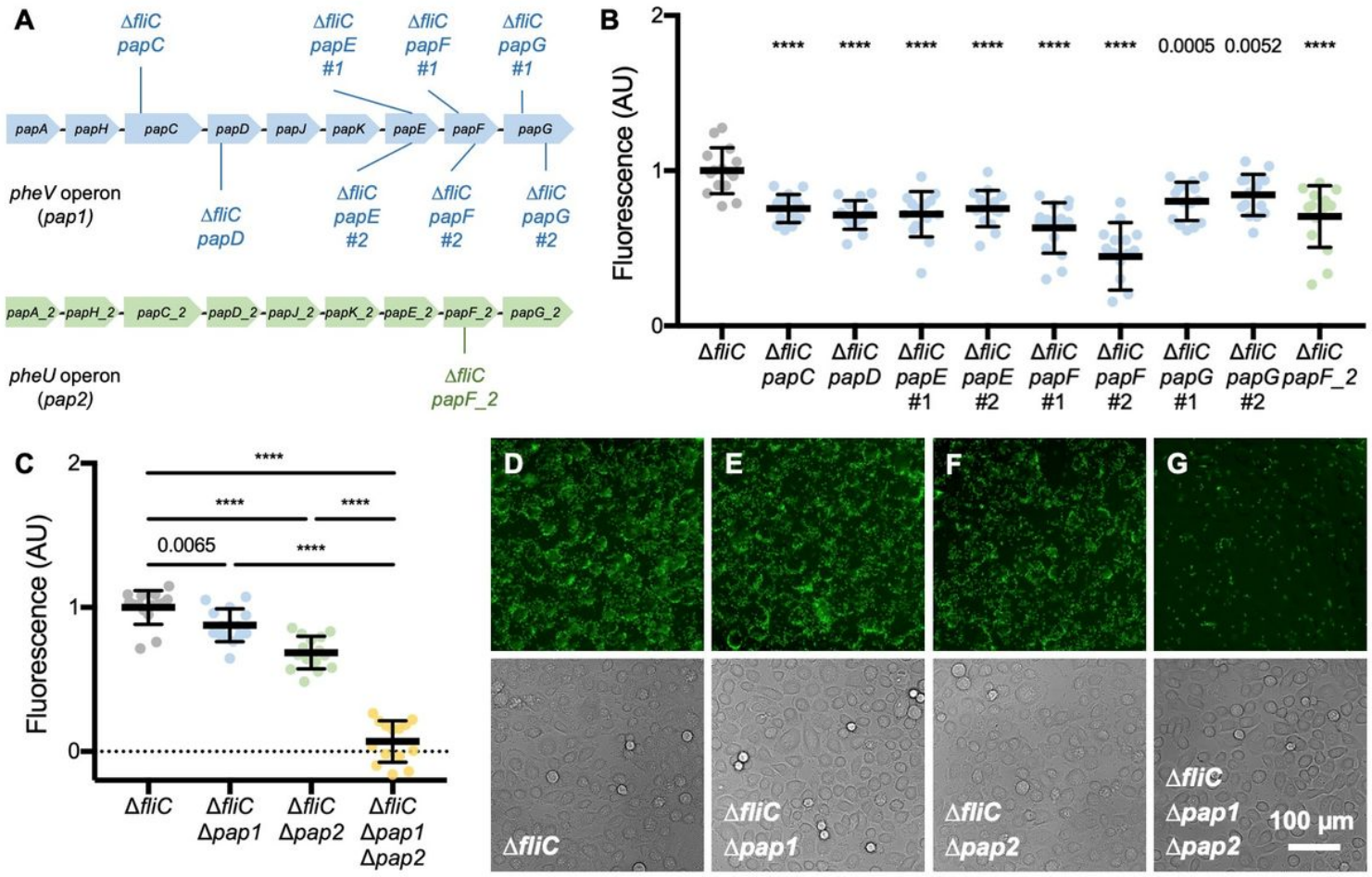

Figure 3

P pili are key mediators of early adhesion of UPEC to bladder epithelial cells. (A) Position of transposon insertions identified within the two P pili operons of CFT073. Top: *pheV*operon (*pap1*, blue). Bottom: *pheU*operon (*pap2*, green). **(B,C)** Quantification of GFP fluorescence after spinfection/washing of bladder epithelial cells with the indicated UPEC strains. n = 15 wells from 3 independent experiments; data were normalized to the Δ*fliC* parental strain; black lines indicate mean and standard deviation; *P*-values were calculated using Welch's t-test, comparing mutant strains to the Δ*fliC* parental strain in **(B)**; **** $P < 0.0001$. **(B)** Cells were infected with *pap1* (blue) or *pap2* (green) transposon mutant strains. Corresponding phase-contrast and green fluorescence images are shown in **Supplementary Figure S4**. **(C)** Cells were infected with unmarked *pap1* (blue), *pap2*(green), or *pap1 pap2* (yellow) deletion mutant strains. **(D-G)** Corresponding phase-contrast and green fluorescence images for the Δ*fliC* parental strain **(D)**, single *pap* deletion mutants Δ*fliC* Δ*pap1* **(E)** and Δ*fliC* Δ*pap2* **(F)**, and double *pap* deletion mutant Δ*fliC* Δ*pap1* Δ*pap2* **(G)**. Scale bar: 100 µm for all images.

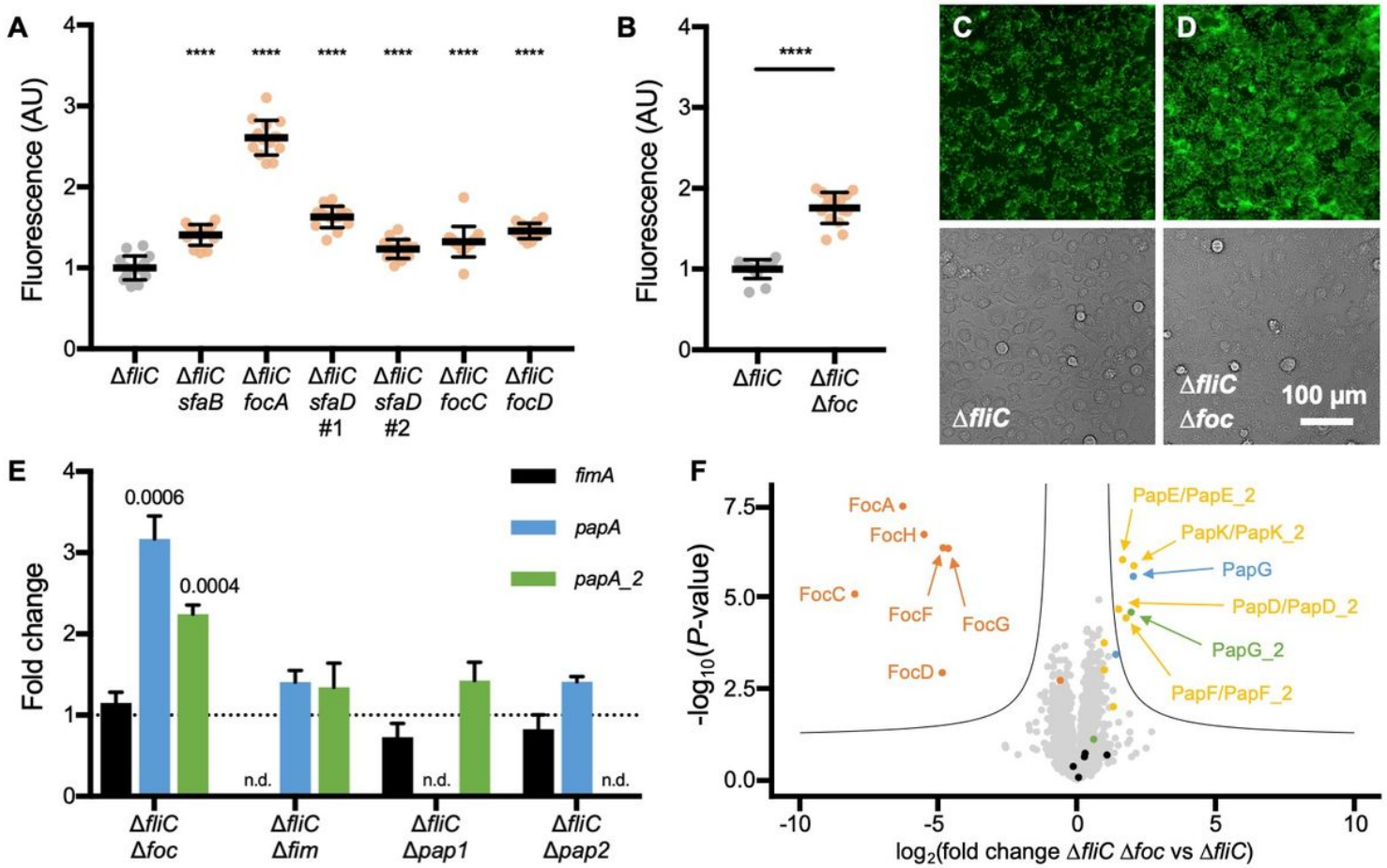

Figure 4

Loss of F1C pili leads to increased P pili expression and increased adhesion of UPEC to bladder epithelial cells. (A,B) Quantification of GFP fluorescence after spinfection/washing of bladder epithelial cells with the indicated UPEC strains. n = 15 wells from 3 independent experiments; data were normalized to the Δ*fliC* parental strain; black lines indicate mean and standard deviation; *P*-values were calculated using Welch's t-test comparing mutant strains to the Δ*fliC* parental strain; **** $P < 0.0001$. **(A)** Cells were infected with *foc* (F1C pili operon) transposon mutant strains (orange). Corresponding phase-contrast and green fluorescence images are shown in **Supplementary Figure S6**. **(B)** Cells were infected with an unmarked *foc* deletion mutant strain (orange). **(C,D)** Corresponding phase-contrast and green fluorescence images for the Δ*fliC*parental strain **(C)** and the Δ*fliC* Δ*foc* mutant strain **(D)**. Scale bar: 100 µm for all images. **(E)** Expression levels of genes encoding the major pilin subunits of type 1 pili (*fimA*, black), P1 pili (*papA*, blue), and P2 pili (*papA_2*, green) measured by qRT-PCR for the indicated mutant strains. Relative expression (fold change) was calculated by normalizing to the Δ*fliC* parental strain. n = 3 independent experiments; bars indicate mean; error bars indicate standard deviation; *P*-values were calculated using Student's t-test comparing mutant strains to the Δ*fliC* parental strain; *P*-values > 0.05 are not shown; n.d. not detected. **(F)** Volcano plot showing changes in surface protein abundances between the Δ*fliC* Δ*foc* mutant strain and the Δ*fliC* parental strain. Proteins that are part of the following pili operons are colored: type 1 pili (black), P1 pili (blue), P2 pili (green), proteins common to P1 and P2 pili (yellow), F1C pili (orange). The name of the proteins showing a significant change is indicated. n = 4

independent experiments; the black line corresponds to a false discovery rate (FDR) of 0.01 and a S0 of 0.5.

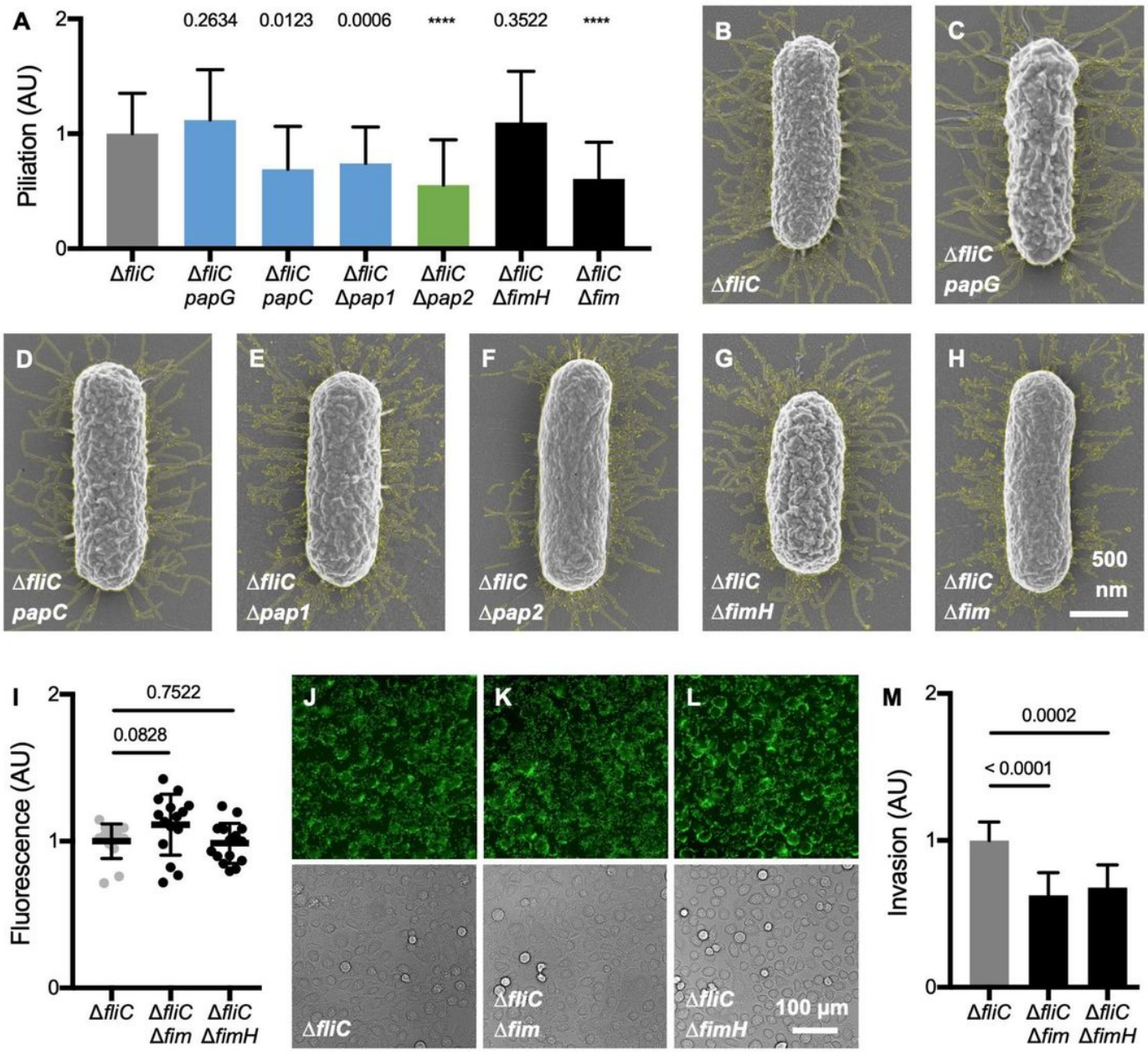

Figure 5

Type 1 pili are not required for early adhesion but are essential for invasion of UPEC into bladder epithelial cells. (A) Quantification of single-cell piliation for the indicated UPEC strains. n ≥ 12 bacteria from 3 independent experiments; data were normalized to the Δ*fliC* parental strain; bars indicate mean; error bars indicate standard deviation; *P*-values were calculated using Mann-Whitney's test comparing mutant strains to the Δ*fliC* parental strain; **** $P < 0.0001$. **(B-H)** Scanning electron micrographs outlining

in yellow the pili identified by the Ilastik-based image analysis pipeline described in **Supplementary Figure S9**. Images show representative bacteria for the Δ*fliC* parental strain **(B)**, Δ*fliC papG*-Tn **(C)**, Δ*fliC papC*-Tn **(D)**, Δ*fliC* Δ*pap1* **(E)**, Δ*fliC* Δ*pap2* **(F)**, Δ*fliC* Δ*fimH* **(G)** and Δ*fliC* Δ*fim* **(H)** mutant strains. Scale bar: 500 nm for all images. **(I)** Quantification of GFP fluorescence after spinfection/washing of bladder epithelial cells with the indicated UPEC strains. n = 15 wells from 3 independent experiments; data were normalized to the Δ*fliC* parental strain; black lines indicate mean and standard deviation; *P*-values were calculated using Welch's t-test. **(J-L)** Corresponding phase-contrast and green fluorescence images for the Δ*fliC* parental strain **(J)**, Δ*fliC* Δ*fim* **(K)** and Δ*fliC* Δ*fimH* **(L)** deletion mutant strains. Scale bar: 100 µm for all images. **(M)** Quantification of bladder cell invasion for the indicated UPEC strains. n = 3 independent experiments; data were normalized to the Δ*fliC* parental strain; bars indicate mean; error bars indicate standard deviation; *P*-values were calculated using Welch's t-test.

Supplementary Files

This is a list of supplementary files associated with this preprint. Click to download.

- SupplementaryFiguresAndTables.docx
- SupptableS1increasedTS.xlsx